JACS
JOURNAL OF THE AMERICAN CHEMICAL SOCIETY

COMMUNICATION

pubs.acs.org/JACS

Visualizing Zeptomole (Electro)Catalysis at Single Nanoparticles within an Ensemble

Stanley C.S. Lai,[†] Petr V. Dudin,[†] Julie V. Macpherson, and Patrick R. Unwin*

Department of Chemistry, University of Warwick, Coventry CV4 7AL, United Kingdom

Supporting Information

ABSTRACT: The relationship between the structural properties, such as the size and the shape, of a catalytic nanoparticle and its reactivity is a key concept in (electro) catalysis. Current understanding of this relationship is mainly derived from studies involving large ensembles of nanoparticles (NPs). However, the results necessarily reflect the average catalytic behavior of an ensemble, even though the properties of individual particles may vary widely. Here, we demonstrate a novel approach using scanning electrochemical cell microscopy (SECCM) to locate and map the reactivity of individual NPs within an electrocatalytic ensemble, consisting of platinum NPs supported on a single carbon nanotube. Significantly, our studies show that subtle variations in the morphology of NPs lead to dramatic changes in (potential-dependent) reactivity, which has important implications for the design and assessment of NP catalysts. The instrumental approach described is general and opens up new avenues of research in functional imaging, nanoscale electron transfer, and catalysis.

A fundamental understanding of processes occurring at supported metal nanoparticles (NPs) is not only of scientific interest, but also technologically relevant, as NPs are employed in many (electro)catalytic processes to optimize metal utilization.[1−4] In particular, the relationship between the size and structure of a NP and its catalytic activity has been studied extensively.[1,5−13] However, as the vast majority of investigations have employed a large number of particles in a catalytic ensemble, the information obtained is limited due to unavoidable variations in NP size, shape, and local environment.[14]

Efforts to circumvent this limitation have been made by shifting to single-particle measurements,[15−20] but such studies are rather challenging.[21] In general, single-particle experiments fall into one of two categories. First, a single NP can be deposited on an electrode with a small surface area, either through electrodeposition[15,16] or through collision of a colloidal NP in solution with the electrode.[17] Valuable insights can be obtained, but such studies preclude an understanding of ensemble behavior and are limited in the range of electrode supports and environments that can be investigated. Second, attempts have been made to study NP ensembles at a single-particle level by scanning probe techniques, such as scanning tunneling microscopy[19] and scanning electrochemical microscopy.[18] However, such studies are complicated by the challenges in locating a NP and in isolating the reactivity of a single NP from the influence of nearby NPs.

The new approach reported herein, using scanning electrochemical cell microscopy (SECCM),[22] allows us to study heterogeneous (electro)catalysis, on a support of any character, shape, and size.

Significantly, we are able to readily locate single NPs, measure their local activity, and map the entire reactivity of a NP ensemble, thereby probing the reactivity of many NPs, each with its own unique characteristics. We thus bridge the gap between (classical) ensemble studies and isolated single NP studies. In particular, this approach allows us to study the effects of NP size, structure, and local support simultaneously during a single experiment, a capability which has not been demonstrated before. To illustrate the new approach, we have studied platinum nanoparticles (Pt-NPs) electrodeposited on an isolated single-walled carbon nanotube (SWNT) grown by chemical vapor deposition as a model system. This system is inspired by the catalysts employed in low-temperature fuel cells, which utilize carbon-supported platinum(-based) nanoparticles for both electrodes. Significantly, we find that individual NPs have their own intrinsic electrochemical characteristics, particularly in the oxygen reduction and hydrogen evolution regions. Such disparities in individual NP reaction rates are clearly important, and we advocate that they need to be taken into account to gain a true picture of NP ensemble behavior.

Electrodeposition on an individual SWNT template produced an ensemble of electrically connected Pt-NPs[23,24] and allowed us to complement SECCM measurements with conventional high-resolution microscopy, enabling direct correlation of reactivity and NP morphology (Figure 1). In addition, electrodeposition circumvents the need for stabilizing ligands which may shield (certain sites) on the NPs for electron transfer. It can be seen clearly in the conventional optical microscope image (Figure 1a) that the sample contains well-dispersed NPs. This finding was confirmed and quantified by atomic force microscopy (AFM) and field emission-scanning electron microscopy (FE-SEM) (Figure 1b,c) which revealed the NPs to be 100 ± 14 nm. These particles have a 'cauliflower'-like morphology due to simultaneous hydrogen evolution at the electrodeposition potential[25] (-1.0 V vs Ag/AgCl for 0.2 s), as well as by agglomeration of smaller crystallites during the electrodeposition.[26,27] Investigation of the catalytic behavior of NP agglomerates is of considerable value as catalyst sintering is a common process that occurs during catalytic runs and is speculated as one of the main causes of fuel cell degradation.[28,29] On the other hand, nanocrystalline morphologies of this type may actually facilitate the oxygen

Received: April 29, 2011
Published: June 14, 2011

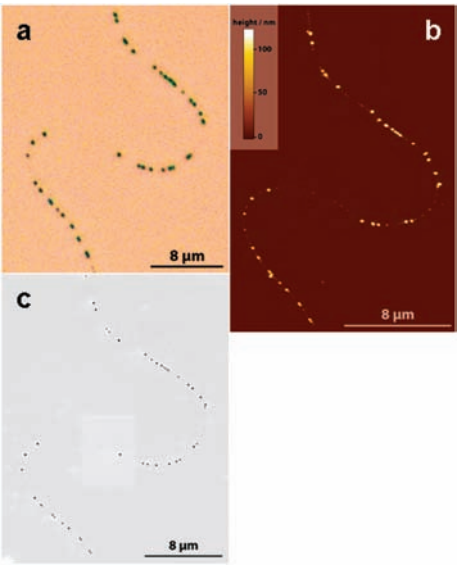

Figure 1. Microscopy images of Pt-NPs on a single carbon nanotube on a SiO_2 substrate. (a) Optical microscopy. (b) AFM. (c) FE-SEM (color inverted for clarity).

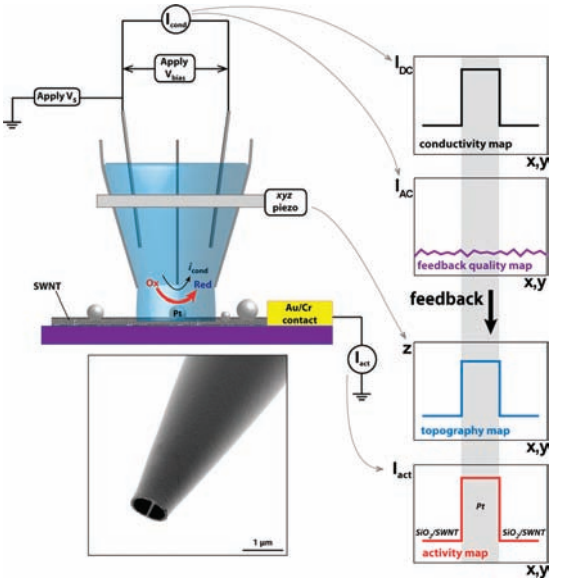

Figure 2. Schematic sketch of a scanning electrochemical cell microscopy (SECCM) experiment. A dual barreled θ pipet pulled to ~1 μm serves as a mobile localized electrochemical cell. The electrolyte solution at the end of the tip is brought into contact with the surface, and a small amplitude oscillation is applied to the z-position of the tip. While scanning in the xy-plane, the ion migration (conductivity) current across the meniscus (I_{cond}), the z-extension of the piezoelectric positioner (z), and the surface activity current (I_{act}) are recorded. The tip−substrate distance is held constant through a feedback mechanism in which the ac-component of the conductivity current (I_{AC}) is maintained at a fixed value. In this way, maps of the dc conductivity (I_{DC}), feedback quality (I_{AC}), topography (z), and surface activity (I_{act}) are obtained simultaneously. (Inset) FE-SEM image of the end of a tip.

reduction reaction,[30] and insights into the behavior of agglomerates (rather than well-dispersed NPs) is of further importance as they are deployed in several important large-scale industrial catalytic processes.[31−34]

The SECCM setup developed and used for electrocatalytic mapping is shown schematically in Figure 2. SECCM provides three simultaneous functional maps of a surface: catalytic activity; topography and conductivity. The probe is a simple dual-channel borosilicate theta pipet, pulled to a sharp taper (~1 μm diameter). Ultimately, the spatial resolution is determined by the tip diameter, and research into smaller tips is ongoing. Each channel was filled with an air-saturated electrolyte solution (0.1 M H_2SO_4), forming a small meniscus at the end of the tip. A palladium−hydrogen (Pd−H_2) quasi-reference electrode (E^0 = 50 mV vs RHE)[35] was inserted into each channel and a fixed potential bias (V_{bias}) of 200 mV applied between the two electrodes, causing a small conductance current (I_{cond}) to flow across the meniscus. The tip was connected to a three-axis (x−y−z) piezoelectric positioner, and a small oscillation (200 nm peak-to-peak amplitude, 83 Hz) was applied to the z-position of the tip. Rough positioning (within 10 μm) of the tip near the point of interest was performed by means of a three-axis micropositioner and video camera monitoring (See Supporting Information). When brought into contact with the sample, I_{cond} develops an alternating current (I_{AC}) component. Using I_{AC} as a set point for the z-position of the tip, a constant tip−sample separation was maintained while scanning the tip in the xy-plane, mapping the topography of the sample. As shown below, changes in the mean conductance current (I_{DC}) allow further unambiguous determination of the location of NPs. Concurrently, the local electrochemical (redox) activity of the substrate is mapped by holding it at the potential of interest (V_s + 1/2 V_{bias} vs Pd−H_2) and measuring the current (I_{act}) passing through it. A data point was typically recorded every micrometer, and the current was averaged over a measurement time of 40 ms at 25 kHz (1000 points). This brief residence time is advantageous in minimizing effects of passification and impurity adsorption from solution. Furthermore, it ensures the interrogation of only the most active sites on a NP; in some cases we were able to measure just a few hundred electrochemical events (zeptomole level detection) when contacting a single NP (*vide infra*). Finally, although the surface is repeatedly wetted and dried, no significant residues were observed with FE-SEM or AFM on the surface after performing SECCM measurements.

Typical SECCM images of the area shown in Figure 1 are shown in Figure 3. Figure 3a−e shows the electrochemical response (I_{act}) of the sample held at various potentials (relative to Pd−H_2). The potentials shown correspond to hydrogen evolution on platinum (−100 mV), oxygen reduction on platinum at different driving forces (100, 300, and 500 mV),[36] and the onset of Pt oxidation (600 mV). Comparing the electrochemical reactivity maps (Figure 3a−e) with the microscopy images of the sample (Figure 1), it is evident that there is excellent correspondence of the electrochemically active regions with the Pt-NPs. Moreover, reactivities as small as 10 fA, corresponding to electroreduction of ~600 O_2 molecules during the 40 ms residence period of the SECCM probe, can be resolved at individual Pt-NPs. It should be noted that the currents observed are significant with respect to the noise levels over the residence period (<30 fA at −100 mV and 100 mV, <3 fA at 300, 500, and 600 mV). Further confirmation that single active particles are identified with this approach comes from the 'topography map' and the mean conductance (I_{DC}), both of which pinpoint the locations of NPs (Figure 3f,g). The set point signal (Figure 3h;

dx.doi.org/10.1021/ja203955b |*J. Am. Chem. Soc.* 2011, 133, 10744–10747

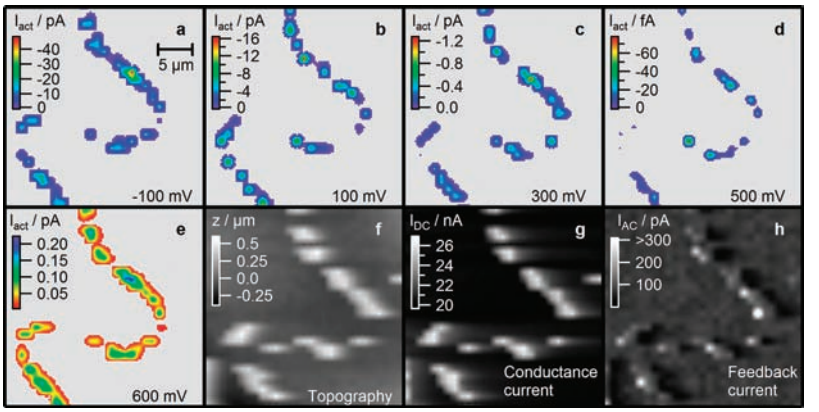

Figure 3. SECCM images of platinum particles deposited on a carbon nanotube of the area shown in Figure 1. (a–e) Electrochemical response (currents) at various potentials, relative to the Pd–H_2 quasi-reference electrode. Note that the currents at 600 mV are oxidative currents. The background current response is displayed in grey for clarity; a full color scale image is included in the Supporting Information. (f) 'Apparent' surface topography. (g) DC conductance current between the two barrels of the SECCM probe. (h) Alternating current (ac) component of the conductance current. (f–h) were recorded at a sample potential of 300 mV.

error image using AFM terminology) likewise highlights morphology changes of the samples.

By examining the SECCM reactivity maps, we can now analyze the behavior of single particles or small groups of particles within a catalytic ensemble as a function of applied potential. Figure 4a shows FE-SEM images of a selection of NPs. 'A'–'C' are single NPs, while 'D' and 'E' consist of two closely spaced NPs which were not resolved individually at the present spatial resolution. Inspecting the current density profiles of the various particles (Figure 4b), using the AFM height data to estimate NP area, four important points are evident. First, the average cathodic current densities observed increase with increasing driving forces (decreasing electrochemical potential) and are generally consistent with literature values,[20] confirming the validity of the measurements. Second, the data for individual NPs display highly nonuniform values. This is clearly illustrated, for example, in the current density profile at 100 mV, where particle 'C' is much more active than others, or at −100 mV where particle 'A' becomes inert (note: I_{DC} proved that particle 'A' was contacted electrochemically). Third, even for particles of similar size based on AFM and FE-SEM (particles 'A' and 'C'), very different reactivity profiles are seen. This is likely related to the more nanofaceted nature of 'C' (evident from the FE-SEM images), which is expected to promote activity.[30] Although most studies only aim to relate reactivity with NP size, this finding clearly demonstrates the importance of considering factors other than particle size. Finally, different (groups of) particles show very different potential–current profiles. While particle 'C' shows the highest current densities (both cathodic and anodic) at all potentials, such trends are less evident for the other particles. For example, particle 'B' shows a comparable reactivity to particle 'C' at −100 mV, but only a fraction of the reactivity at all other potentials. Similarly, the activity of the two particles 'D' at −100 mV and 300 mV is about the same as the average activity (as given by the dashed line in the figure) but is significantly below average at the other potentials. We resolve such large potential-dependent variations in activity (which have also been seen in other electrochemical systems when investigated at the microscale)[37] in part, by virtue of the short residence time and high mass transport rates of the SECCM system.

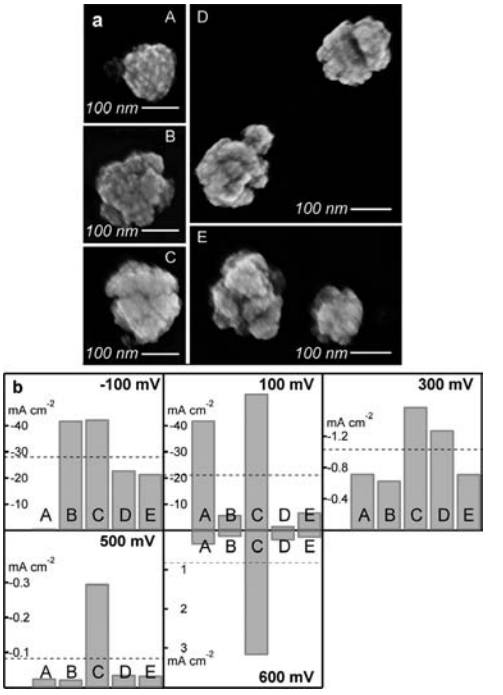

Figure 4. Activity of selected (groups of) particles. (a) High-resolution FE-SEM images of selected example (groups of) particles from the array shown in Figures 1 and 3. (b) Current density plots at various potentials (relative to the Pd–H_2 quasi-reference electrode) for the selected (groups of) particles. Note that the currents at 600 mV are oxidative currents. Current density was calculated on the basis of spherical particles using AFM particle heights (which were similar to the widths from FE-SEM). The dashed line in each plot corresponds to the average current density at that potential.

In summary, the SECCM technique described herein allows reactivity mapping of a complete NP ensemble with single NP resolution. By employing SECCM on a model system comprising electrodeposited platinum NPs on a single walled carbon nanotube, the reactivity of individual NPs has been resolved, revealing unique information on the wide dispersion of reactivity within the ensemble and demonstrating a variance in reactivity

among apparently similarly sized NPs. These results have highlighted the importance of factors other than NP size effects, such as the morphology and local support in determining NP reactivity, an understanding which has remained elusive in previous NP studies. We believe the SECCM method to be a versatile approach toward a full quantitative understanding of NP reactivity. Finally, we emphasize that, although this paper has focused on electrocatalytic reactions, the approach is more general and could be extended to study other heterogeneous systems where the reaction causes a change in conductivity current that can be detected by SECCM. Furthermore, we believe there are prospects to enhance the spatial resolution by an order of magnitude, through the use of smaller probes, which would reduce the need for model systems with widely spaced active sites, as well as further expand the range of systems to which the technique is applicable.

■ ASSOCIATED CONTENT

Supporting Information. Experimental section, illustration of tip positioning and full color scale image of Figure 3. This material is available free of charge via the Internet at http://pubs.acs.org.

■ AUTHOR INFORMATION

Corresponding Author
p.r.unwin@warwick.ac.uk

Author Contributions
†These authors contributed equally to this work

■ ACKNOWLEDGMENT

This work was supported by the Engineering and Physical Sciences Research Council (EPSRC), the Science City Research Alliance-Hydrogen Energy Project and the European Research Council (Advanced Investigator Grant 'QUANTIF'). We gratefully acknowledge fruitful discussions with, and technical support from, Mr. Neil Ebejer, Dr. Alex Colburn, and Dr. Aleix Guëll.

■ REFERENCES

(1) Somorjai, G. A. *Science* **1985**, *227*, 902.
(2) Daniel, M.-C.; Astruc, D. *Chem. Rev.* **2003**, *104*, 293.
(3) Chen, A.; Holt-Hindle, P. *Chem. Rev.* **2010**, *110*, 3767.
(4) Xu, W. L.; Shen, H.; Liu, G. K.; Chen, P. *Nano Res.* **2009**, *2*, 911.
(5) Xu, Z.; Xiao, F. S.; Purnell, S. K.; Alexeev, O.; Kawi, S.; Deutsch, S. E.; Gates, B. C. *Nature* **1994**, *372*, 346.
(6) Sánchez-Sánchez, C. M.; Solla-Gullon, J.; Vidal-Iglesias, F. J.; Aldaz, A.; Montiel, V.; Herrero, E. *J. Am. Chem. Soc.* **2010**, *132*, 5622.
(7) Tian, N.; Zhou, Z. Y.; Sun, S. G.; Ding, Y.; Wang, Z. L. *Science* **2007**, *316*, 732.
(8) Ahmadi, T. S.; Wang, Z. L.; Green, T. C.; Henglein, A.; ElSayed, M. A. *Science* **1996**, *272*, 1924.
(9) Sun, Y. G.; Xia, Y. N. *Science* **2002**, *298*, 2176.
(10) Burda, C.; Chen, X.; Narayanan, R.; El-Sayed, M. A. *Chem. Rev.* **2005**, *105*, 1025.
(11) Ortalan, V.; Uzun, A.; Gates, B. C.; Browning, N. D. *Nat. Nanotechnol.* **2010**, *5*, 843.
(12) Vajda, S.; Pellin, M. J.; Greeley, J. P.; Marshall, C. L.; Curtiss, L. A.; Ballentine, G. A.; Elam, J. W.; Catillon-Mucherie, S.; Redfern, P. C.; Mehmood, F.; Zapol, P. *Nat. Mater.* **2009**, *8*, 213.
(13) Greeley, J.; Rossmeisl, J.; Hellmann, A.; Nørskov, J. K. *Z. Phys. Chem.* **2007**, *221*, 1209.
(14) Hashmi, A. S. K.; Hutchings, G. J. *Angew. Chem., Int. Ed.* **2006**, *45*, 7896.
(15) Krapf, D.; Wu, M.-Y.; Smeets, R. M. M.; Zandbergen, H. W.; Dekker, C.; Lemay, S. G. *Nano Lett.* **2005**, *6*, 105.
(16) Chen, S.; Kucernak, A. *J. Phys. Chem. B* **2003**, *107*, 8392.
(17) Xiao, X. Y.; Bard, A. J. *J. Am. Chem. Soc.* **2007**, *129*, 9610.
(18) Tel-Vered, R.; Bard, A. J. *J. Phys. Chem. B* **2006**, *110*, 25279.
(19) Meier, J.; Friedrich, K. A.; Stimming, U. *Faraday Discuss.* **2002**, *121*, 365.
(20) Chen, S.; Kucernak, A. *J. Phys. Chem. B* **2004**, *108*, 3262.
(21) Bard, A. J. *J. Am. Chem. Soc.* **2010**, *132*, 7559.
(22) Ebejer, N.; Schnippering, M.; Colburn, A. W.; Edwards, M. A.; Unwin, P. R. *Anal. Chem.* **2010**, *82*, 9141.
(23) Quinn, B. M.; Dekker, C.; Lemay, S. G. *J. Am. Chem. Soc.* **2005**, *127*, 6146.
(24) Day, T. M.; Unwin, P. R.; Wilson, N. R.; Macpherson, J. V. *J. Am. Chem. Soc.* **2005**, *127*, 10639.
(25) Penner, R. M. *J. Phys. Chem. B* **2002**, *106*, 3339.
(26) Bayati, M.; Abad, J. M.; Nichols, R. J.; Schiffrin, D. J. *J. Phys. Chem. C* **2010**, *114*, 18439.
(27) Jeon, H.; Joo, J.; Kwon, Y.; Uhm, S.; Lee, J. *J. Power Sources* **2010**, *195*, 5929.
(28) Wilson, M. S.; Garzon, F. H.; Sickafus, K. E.; Gottesfeld, S. *J. Electrochem. Soc.* **1993**, *140*, 2872.
(29) Mamat, M. S.; Grigoriev, S. A.; Dzhus, K. A.; Grant, D. M.; Walker, G. S. *Int. J. Hydrogen Energy* **2010**, *35*, 7580.
(30) Komanicky, V.; Menzel, A.; You, H. *J. Phys. Chem. B* **2005**, *109*, 23550.
(31) Devred, F.; Gieske, A. H.; Adkins, N.; Dahlborg, U.; Bao, C. M.; Calvo-Dahlborg, M.; Bakker, J. W.; Nieuwenhuys, B. E. *Appl. Catal. A* **2009**, *356*, 154.
(32) Schlogl, R. *Angew. Chem., Int. Ed.* **2003**, *42*, 2004.
(33) Erisman, J. W.; Sutton, M. A.; Galloway, J.; Klimont, Z.; Winiwarter, W. *Nat. Geosci.* **2008**, *1*, 636.
(34) Huber, G. W.; Iborra, S.; Corma, A. *Chem. Rev.* **2006**, *106*, 4044.
(35) Vasile, M. J.; Enke, C. G. *J. Electrochem. Soc.* **1965**, *112*, 865.
(36) Gewirth, A. A.; Thorum, M. S. *Inorg. Chem.* **2010**, *49*, 3557.
(37) Basame, S. B.; White, H. S. *Anal. Chem.* **1999**, *71*, 3166.